

See discussions, stats, and author profiles for this publication at: <https://www.researchgate.net/publication/322309601>

# Identification of Quadrotor Aerodynamic Model from High Speed Flight Data

Conference Paper · January 2018

DOI: 10.2514/6.2018-0523

---

CITATIONS

6

READS

2,787

3 authors:



Sihao Sun

Delft University of Technology

13 PUBLICATIONS 62 CITATIONS

[SEE PROFILE](#)



Rudi Schilder

Delft University of Technology

1 PUBLICATION 6 CITATIONS

[SEE PROFILE](#)



Coen De Visser

Delft University of Technology

157 PUBLICATIONS 1,203 CITATIONS

[SEE PROFILE](#)

Some of the authors of this publication are also working on these related projects:



Innovative Control Methods to Reduce Pilot Workload in Tiltrotor Aircraft [View project](#)



Drone fault tolerant control [View project](#)



# Identification of Quadrotor Aerodynamic Model from High Speed Flight Data

S. Sun,\* R. J. Schilder,† C.C. de Visser‡

Delft University of Technology, 2629HS Delft, The Netherlands

In order to fill the gap of knowledge about the aerodynamic effects of a quadrotor in aggressive flight conditions, identification of the aerodynamic forces and moments occurring during high speed flight are performed. A gray-box model is established as a mapping from states, rotor speeds to resultant forces and moments. Prior knowledge about quadrotor aerodynamics together with a stepwise regressor selector is applied to identify the model structure. Data for this research is obtained from free flight tests in the Open Jet Facility (wind tunnel) of the TU Delft, with wind speeds up to 14m/s. State information is inferred from inertial on-board sensors and Motion Capture cameras. Moments produced by aerodynamic effects have been observed and precisely modeled. During validation, the new model showed superior prediction performance when compared to current models that neglect fast flight aerodynamic effects.

## Nomenclature

$u$	velocity x component on body frame, m/s
$v$	velocity y component on body frame, m/s
$w$	velocity w component on body frame, m/s
$p$	rolling rate, rad/s
$q$	pitching rate, rad/s
$r$	yawing rate, rad/s
$V$	airspeed, m/s
$\alpha$	angle of attack, rad
$\beta$	sideslip angle, rad
$\nu_i$	rotor induced velocity, m/s
$\nu_h$	rotor induced velocity during hover, m/s
$\vec{F}$	resultant force vector except gravity, N
$\vec{M}$	resultant moment vector, Nm
$\mathbf{I}_v$	inertia matrix of the vehicle, $\text{kgm}^2$
$I_{r,z}$	rotor moment of inertia that perpendicular to the rotor disk, $\text{kgm}^2$
$R$	rotor radius, m
$\vec{F}_a$	aerodynamic force vector, N
$\vec{F}_r$	reduced model of resultant force vector except gravity, N
$\vec{M}_a$	aerodynamic moment vector, Nm
$\vec{M}_r$	resultant moment vector of reduced model, Nm
$T$	total thrust, N
$T_h$	total thrust during hover, N
$\rho$	air density, $\text{kg/m}^3$

\*Ph.D. student, Control and Simulation Division, Faculty of Aerospace Engineering, Kluyverweg 1, 2629HS Delft, The Netherlands; s.sun-4@tudelft.nl

†Graduate student, Control and Simulation Division, Faculty of Aerospace Engineering, Kluyverweg 1, 2629HS Delft, The Netherlands; rudi.schilder@gmail.com

‡Assistant professor, Control and Simulation Division, Faculty of Aerospace Engineering, Kluyverweg 1, 2629HS Delft, The Netherlands. AIAA Member

$\omega_i$	rotation speed of <i>i</i> th rothr, rad/s
$U_p$	rotor speed combinations for roll control $U_p = \omega_1^2 - \omega_2^2 - \omega_3^2 + \omega_4^2$ , (rad/s) <sup>2</sup>
$U_q$	rotor speed combinations for pitch control $U_p = \omega_1^2 + \omega_2^2 - \omega_3^2 - \omega_4^2$ , (rad/s) <sup>2</sup>
$U_r$	rotor speed combinations for yaw control $U_p = \omega_1^2 - \omega_2^2 + \omega_3^2 - \omega_4^2$ , (rad/s) <sup>2</sup>
$\kappa_0$	thrust coefficient during hover
$\tau_0$	torque coefficient during hover
$A$	regressor matrix
$z$	measurements
$\theta_i$	coefficient of the <i>i</i> th regressor
$\hat{\theta}_i$	estimation of the coefficient of the <i>i</i> th regressor
$\lambda_i$	portion of the <i>i</i> th candidate regressor participating in stepwise selection process.
$\epsilon$	residuals of model
$\xi_i$	the <i>i</i> th regressor
$F_0$	partial F-ratio
$N$	data length
$P^d$	dth order polynomial function
<i>Subscript</i>	
<i>i</i>	Rotor index / Variable number

## I. Introduction

Multi rotor drones are increasingly popular with new applications emerging virtually every day. With respect to out-door environments, drones are being used for delivery, reconnaissance, infrastructures inspection and more. These drones are frequently operating in a high speed flight conditions, while facing non-negligible aerodynamic effects.

Drones can successfully operate in these conditions using their sensors and high bandwidth control systems to counter the lack of a full envelope model and attain their objectives. However the often simplified aerodynamics in these conditions are non-negligible and add large disturbances to the expected system dynamics. By investigating the aerodynamic effects and modeling them to their full extent, this can lead to more optimized controllers and deep understanding of drone behavior in aggressive flights.

The quadrotor drone is one of the most widely used multi rotor drones, and is the subject of this research. The motion of quadrotors has primarily been described by rigid body 6-DOF models experiencing a set of external forces and moments, where the aerodynamic effects play a key role. Rotors are the primary components that generate forces and moments. From previous literatures that use helicopter momentum and blade element theory, it can be concluded that at least three different phenomenon have a significant effect. Firstly, the thrust is susceptible to the incoming flow velocity, especially during climbing and descending flight.<sup>6,19</sup> Secondly blade flapping occurs, resulting in an inclined rotor disk plane, producing a local drag force and elastic moment.<sup>15</sup> Thirdly hub force occurred due to induced drag produced by rotor blades.<sup>15</sup>

First principle based models are established, taking above aerodynamic effects into account. Drag model derived from blade element theory is involved into many researches.<sup>13–16</sup> These drag models possess high prediction accuracy. However, the complex aerodynamic interactions between rotors are not considered. Thrust variance model during climbing and descending flight are also successfully predicted by first principle approaches.<sup>6,19</sup> However, Due to the complexity of computing induced velocity and aerodynamic interactions, the existing first principle based model are unable to provide accurate thrust predictions in forward flight,<sup>19</sup> not to mention coupled flight states in which lateral and longitudinal maneuver occur simultaneously.

Furthermore, the pitch (roll) and yaw moment model in a fast flight condition are less discussed compared to drag and thrust models. Moment models derived from blade element theory<sup>16</sup> and blade flapping effects<sup>1,6</sup> have been discussed however not validated in these literatures, thus lack of evidence of their availability is given.

Parameters of these existing models can be acquired by direct measurements or system identification technique. However, the model structure in those models are determined merely from physical knowledge derived from helicopter theories, which may lose their feasibility for multi rotor vehicles. An alternative approach for establishing the model structure is an data driven stepwise structure selection method,<sup>11</sup> which requires a group of candidate structure elements in a polynomial form. These elements are named regressors

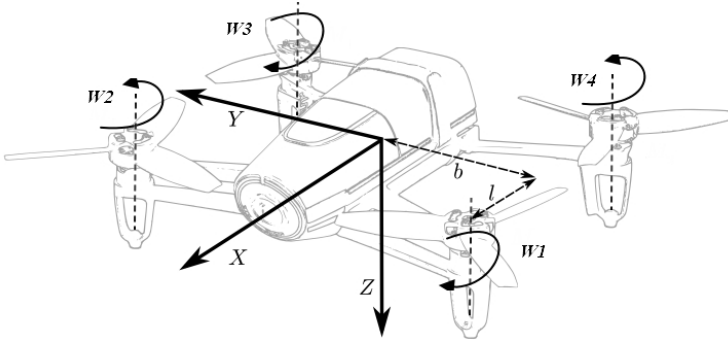


Figure 1: Body axis definition and Bebop quadrotor rotor rotation directions<sup>20</sup>

since regression method, such as Least Square Regression, is used to determine their coefficients. The candidate regressors can be chosen based on prior-knowledge, observations or assumptions. Since both prior-knowledge and real life observation are considered, this type of modeling approach is suitable for systems with both known and unknown effects. This "gray-box" approach is widely used for full-scale aircrafts,<sup>2, 4, 10, 11, 22, 23</sup> however hasn't been seen in any applications for quadrotors.

There are two main outputs of this research with the use of gray-box system identification approach. Firstly, global models for thrust and drag considering coupling effects between lateral and longitudinal motions are established. Secondly, strong aerodynamic moments during fast forward flight were observed and modeled. Assumption was made based on this observation that the aerodynamic moment was caused by interaction effect between rotors. These models could be helpful for the future usage of simulation, controller design or performance analysis of specific quadrotor. It is finally shown that the new aerodynamic model provides accurate prediction especially during high speed flight conditions.

Flight data used for system identification were collected in the Open Jet Facility of TU Delft, a low-speed large cross section wind tunnel. Free flight tests trying to explore the full flight envelope were made for global model establishment. IMU (Inertia Measurement Units) provided resultant forces and moments measurements indirectly, while other states such as attitude and velocity were obtained by a motion capture system.

This paper is organized as follows. Chapter II gives the reduced model as a benchmark for comparison. Chapter III introduces the method of system identification. Chapter IV describes the experiment setup and data gathering and after which, Chapter V will derive the model structure of aerodynamic force and moment models. Chapter VI will demonstrate the modeling result and discuss the observed phenomena. Lastly the conclusions and recommendations are given in Chapter VII.

## II. Reduced Model

To further elaborate the aerodynamic model of quadrotor, the reduced model is introduced as a benchmark. This model is widely used for designing controller for hovering flights, but is unsuitable for flights with even slight translational velocities.

First of all, the body reference definition is given in Fig 1 , where  $x$  axis points forward and  $z$  axis points downward, and origin in the center of gravity . By regarding quadrotor as a rigid body, dynamic equations are shown in Eq 1 and 2

$$m \begin{bmatrix} \dot{u} \\ \dot{v} \\ \dot{w} \end{bmatrix} = m \begin{bmatrix} p \\ q \\ r \end{bmatrix} \times \begin{bmatrix} u \\ v \\ w \end{bmatrix} + \vec{G} + \vec{F} \quad (1)$$

$$\mathbf{I}_v \begin{bmatrix} \dot{p} \\ \dot{q} \\ \dot{r} \end{bmatrix} = \begin{bmatrix} p \\ q \\ r \end{bmatrix} \times \mathbf{I}_v \begin{bmatrix} p \\ q \\ r \end{bmatrix} + \vec{M} \quad (2)$$

where  $u, v, w$  indicate the velocity components expressed in body reference, and  $p, q, r$  stand for angular speed with respect to the three axis.  $m$  and  $\mathbf{I}_v$  represent mass and inertia matrix respectively.  $\vec{G}$  is gravity

vector.  $\vec{F}$  is the resultant force except gravity and  $\vec{M}$  indicates the resultant moment on quadrotor. The above dynamic equations hold no matter whether aerodynamic effect is included.

Emphasis is placed on the modeling of forces and moments. The resultant force equals

$$\vec{F} = \vec{F}_r + \vec{F}_a \quad (3)$$

where

$$\vec{F}_r = \begin{bmatrix} 0 \\ 0 \\ -T_h \end{bmatrix} = \begin{bmatrix} 0 \\ 0 \\ -\kappa_0 \sum \omega_i^2 \end{bmatrix} \quad (4)$$

is regarded as the reduced model of forces, which holds in hover condition.  $T_h$  represents the resultant rotor thrust force during hovering flight.  $\omega_i$  indicates the  $i$ th rotor's angular speed.  $\kappa_0$  is a coefficient related to rotor property and air density and is regarded as a constant for drone's rotor. Just as its name implies, the reduced model is too simple to fit the model in flights out of hover conditions, where additional forces related to aerodynamic effects play important roles. Therefore, we add a second term in Eq 4,  $\vec{F}_a$ , which stands for the translational speed related aerodynamic forces.

As for the resultant moment, it equals

$$\vec{M} = \vec{M}_r + \vec{M}_a \quad (5)$$

$\vec{M}_r$  indicates the reduced moment model in which complex aerodynamic effects are neglected, and is expressed as

$$\vec{M}_r = \begin{bmatrix} b\kappa_0 U_p + qI_{r,z}(-\omega_1 + \omega_2 - \omega_3 + \omega_4) \\ l\kappa_0 U_q + pI_{r,z}(\omega_1 - \omega_2 + \omega_3 - \omega_4) \\ \tau_0 U_r + I_{r,z}(-\dot{\omega}_1 + \dot{\omega}_2 - \dot{\omega}_3 + \dot{\omega}_4) \end{bmatrix} \quad (6)$$

where  $U_p = \omega_1^2 - \omega_2^2 - \omega_3^2 + \omega_4^2$ ,  $U_q = \omega_1^2 + \omega_2^2 - \omega_3^2 - \omega_4^2$ , and  $U_r = \omega_1^2 - \omega_2^2 + \omega_3^2 - \omega_4^2$ . They represent the combinations of rotor speeds for roll, pitch, yaw control respectively.  $b$  and  $l$  are distance from c.g to rotor centers in x and y direction.  $\tau_0$  is a coefficient for drag moment, and is regarded as a constant.  $I_{r,z}$  is the z direction moment of inertia of single rotor. The first term in each component of  $\vec{M}_r$  is from rotor thrust and rotor drag, and the second terms are caused by rotor inertia effects (gyroscope effect and inertia torque).  $\vec{M}_a$  is the moment caused by aerodynamic effects in flights with translational motions and is rarely discussed. However, from our research, the aerodynamic effect is playing a significant role and unable to be eliminated even in a relatively slow flight.

In order to establish the global model of quadrotor in fast forward flight, the main focus of this paper is to apply system identification technique to find the model of  $\vec{F}$  and  $\vec{M}$  which contain  $\vec{F}_a$  and  $\vec{M}_a$ .

### III. Methodology

This chapter will introduce the system identification method applied in this paper. Specifically, a regression method together with gray-box model structure selection method is used for modeling the aerodynamic forces and moments. Here model denotes a mapping from independent variables, i.e quadrotor states and rotor speeds to moment and forces acting on it. The regression model is in the form

$$z = A\theta + \epsilon \quad (7)$$

where  $z \in R^N$  stands for  $N$  measurement data.  $A = [1, \xi_1, \xi_2 \dots \xi_p] \in R^{N \times p}$  indicates regressors matrix with a constant vector in the first column.  $\xi_i$  represents regressor which is an arbitrary combination of independent variables, e.g. power series.  $\theta \in R^p$  stands for parameters corresponding to the regressors.  $A\theta$  represents model output and here  $\epsilon \in R^n$  vector stands for residual between real measurement and model output in each data point. Original least square (OLS) method is used for determining the parameters

$$\hat{\theta} = (A^T A)^{-1} A^T z \quad (8)$$

where  $\hat{\theta}$  is the optimal parameter estimate that minimize the residual  $\epsilon$ . Now, how to determine the regressors contained in the model Eq 7 becomes the main concern. This procedure is called model structure selection.

In this paper, two steps are used for selecting model structure. The first step is using prior first principles knowledge to narrow search range of potential model structures as well as finding independent variables in a specific model. It is possible to find comparatively good force model structure from helicopter aerodynamics. For moment model, the mechanics behind it has not been researched adequately, due to complex interactions between rotors. However, there are still theories and observed phenomenon helping us to find a preliminary model structure. The preliminary model will contain undetermined parts to be selected in the next step.

The second step is called forward-backward stepwise model structure selection. It is an algorithm for determining specific model structure from abundant candidate regressors formed by determined independent variables and is well elaborated in Ref. 11, but will be briefly introduced in section III.A. Above structure selection process includes the physical knowledge about the model, as well as the automatic selection procedure based on observation data. Thus the model structure of this gray-box model can be more reliable.

To sum up, there are five steps in this identification process:

1. Flight test and data preprocessing.
2. Preliminary model structure analysis based on first principles.
3. Model structure selection using stepwise method.
4. Parameter estimation by least square method.
5. Model validation

As for flight test and data processing, it will be introduced in Chapter IV. And model validation result will be given in Chapter VI.

### III.A. Stepwise Model Structure Selection

The main goal of structure selection process is finding specific regressors from a regressors candidate pool, to form up the final model. The candidate pool consists of possible combinations of independent variables. These combination could be, for example, log function, exponent function, etc. In this paper, polynomial functions have been chosen. For instance, if the preliminary model structure is organized as Eq 9 from prior knowledge

$$y = P_1^2(x_1, x_2) + P_2^2(x_1, x_2)x_3 \quad (9)$$

where  $P^2(x_1, x_2)$  stands for the second order polynomial function formed by  $x_1$  and  $x_2$ . Then the candidate pool contains all kinds of combinations of independent variables. In this example, candidates should be  $x_1, x_2, x_3, x_1^2, x_2^2, x_1x_2$  and  $x_1x_3, x_2x_3, x_3x_3, x_1^2x_3, x_2^2x_3, x_1x_2x_3$ . Generally, for a  $d$ th order polynomial function with  $n$  independent variables  $P^d(x_1, x_2, \dots, x_n)$ , the total number of terms in the candidate pool is<sup>3</sup>

$$\hat{d} = \frac{(d+n)!}{n!d!} \quad (10)$$

After defining the candidate pool, the forward-backward stepwise selection process is described in following steps to select qualified regressors to form up the model.<sup>11</sup>

- Initialization:  
The model starts from the simplest form with only constant term

$$z = A\theta_0 + \epsilon, \quad A = \begin{bmatrix} 1 \\ \vdots \\ 1 \end{bmatrix} \quad (11)$$

- Loop:

1. Estimate parameters in the model by Eq 8. And compute the model residual by

$$\epsilon = z - A\hat{\theta} \quad (12)$$

2. For each candidate regressor in the pool, remove part of it until the rest is orthogonal to the terms already in the model. This process is achieved by using least square method. Specifically, for regressor  $\xi_i$  in the pool, the rest part after this removal equals

$$\lambda_i = \xi_i - A(A^T A)^{-1} A^T z \quad (13)$$

3. Select the index  $j$  with which  $\lambda_j$  has the highest correlation with current model residual  $\epsilon$ . Add candidate  $\xi_j$  into the model as a new column of regressor matrix  $A$ .
4. Evaluate existing regressors in the model by F test. Assume there are already  $p$  regressors in the current model. The partial F-ratio for the  $k$ th regressor is

$$F_0 = \frac{SS_R(\hat{\theta}_p) - SS_R(\hat{\theta}_{p-k})}{s^2} \quad (14)$$

where  $s^2$  is fit error variance computed by

$$s^2 = \frac{\epsilon^T \epsilon}{N - p - 1} \quad (15)$$

$SS_R(\hat{\theta}_p)$  stands for the regression sum of squares for current model, and  $SS_R(\hat{\theta}_{p-k})$  stands for that of the model after eliminating the regressor  $\xi_k$ . The formula for regression sum of squares is

$$SS_R = \hat{\theta}^T A^T z - N\bar{z} \quad (16)$$

where  $\bar{z}$  is the mean of measurement  $z$ . If  $\xi_i$  is the regressor with the least  $F_0$  and

$$F_0 < F_{out} \quad (17)$$

then this regressor is eliminated from the current model.  $F_{out}$  can be taken as a constant equals to 4. If  $\xi_k$  is exactly the regressor selected in the last step, algorithm stops.

- Stopping Criterion:

Predict square error (PSE) could be used as the stopping criterion in this algorithm.

$$PSE = \frac{1}{N} \epsilon^T \epsilon + \sigma_{max}^2 \frac{p}{N} \quad (18)$$

The first term is the mean square fit error for the modeling data, and the second term is the penalty term for model redundancy. The penalty coefficient is chosen as

$$\sigma_{max}^2 = \frac{1}{N} \sum_{i=1}^N [z(i) - \bar{z}]^2 \quad (19)$$

More regressors in the model, i.e larger  $p$ , the penalty term will contribute more for PSE. Thus as there are more regressors added into the model, the PSE will decrease at the beginning and finally increase. Thus if

$$PSE \geq PSE_{last} \quad (20)$$

the algorithm stops to avoid over-fitting.

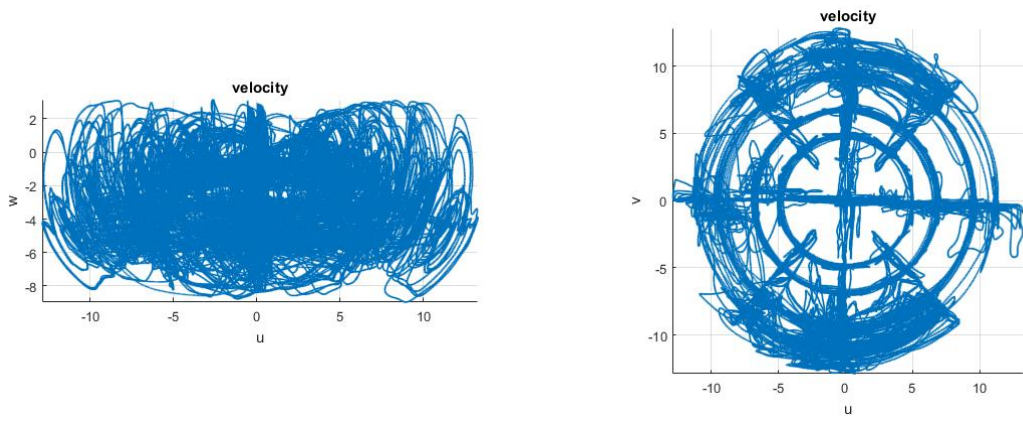
## IV. Experimental Setup

### IV.A. Platform

The selected experimental platform is the Parrot Bebop, a quadrotor equipped with an integrated camera for photos and videos. The native software is replaced by Paparazzi, an open-source autopilot platform. The autopilot runs on a 512Hz loop, estimating the state using its various sensors, sending control commands and logging desired information.



Figure 2: Flight test in Open Jet Facility, Delft University of Technology



(a) Flight trajectory in  $u - w$  plane

(b) Flight trajectory in  $u - v$  plane

Figure 3: Flight trajectory expressed in velocity space.

The sensors available to the Bebop quadrotor include: 3-axes accelerometer (MPU 6050), 3-axes gyroscope (MPU 6050), 3-axes magnetometer (AKM 8963), closed loop rpm controlled brushless rotors with back-EMF rotor rate feedback. During the experiment, the accelerometer, gyroscope and rotor rate values are logged at 512Hz.

Using the mass and simple inertia estimates of individual components, a estimate of the inertias was established. The results are shown in Table 1. The process is described in Ref. 17, where the inertias are determined for a similar quadrotor and validated withing a 5% accuracy. It is expected that this error will only influence the value of resulting regressors coefficients and will not significantly influence the selection of these regressors.

Table 1: Mass property estimation of tested quadrotor

Mass[ $kg$ ]	$I_{xx}[kg \cdot m^2]$	$I_{yy} [kg \cdot m^2]$	$I_{zz} [kg \cdot m^2]$	$I_{xz}[kg \cdot m^2]$
0.38905	0.000906	0.001242	0.002054	1.4178e-05

The flight test was performed in Open Jet Facility (OJF) of Delft University of Technology, as shown in Fig2. The outlet size of this wind tunnel is 3m in diameter, thus there was a space in around 2.5m by 2.5m by 5.0m for the flight test. Due to the thrust limitation of Parrot Bebop, maximum tested wind speed was 14m/s. Incremental Nonlinear Dynamics Inversion (INDI) guidance law<sup>21</sup> and controller<sup>20</sup> were used for tracking desired position and stabilizing attitude in the wind tunnel. Different types of maneuvers were

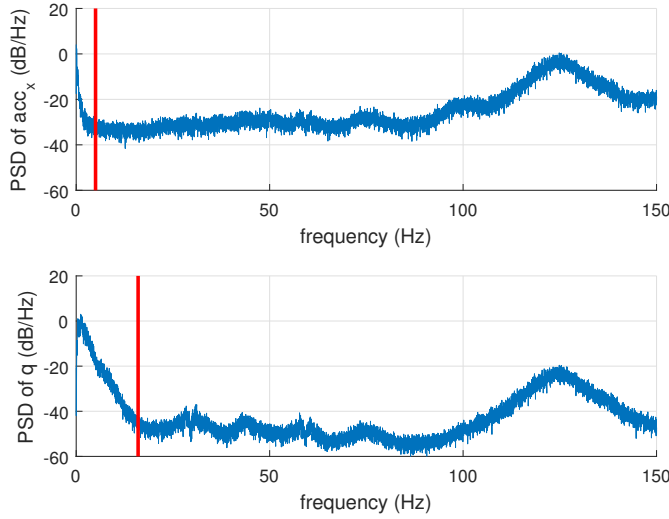


Figure 4: PSD (Power spectral density) estimation of gyroscope and accelerometer measurements. Vertical red lines indicate cut-off frequencies.

implemented for system excitation: maneuvers along wind flow, horizontal maneuver perpendicular to wind flow, climbing and descend flight, yaw maneuver. Except the yaw maneuver, each type of maneuver was finished in different heading angles for identifying coupling effect brought by simultaneous longitudinal and lateral motions. Finally, data covering more than 4000 seconds' flight were used for model identification. Figure 3 shows the flight regime in the  $u - w$  and  $u - v$  plane.

#### IV.B. Data Acquisition and Processing

Optitrack motion capture system was used for providing position, velocity and attitude information. Accelerometer and gyroscope provide specific forces and angular rates respectively. In order to be tracked by motion capture system information, 6 Markers were attached to the quadrotor at various locations: 4 in the hub of rotors and two on the frame.

The accelerometer and gyroscope measurements were used for calculating forces and moments acted on

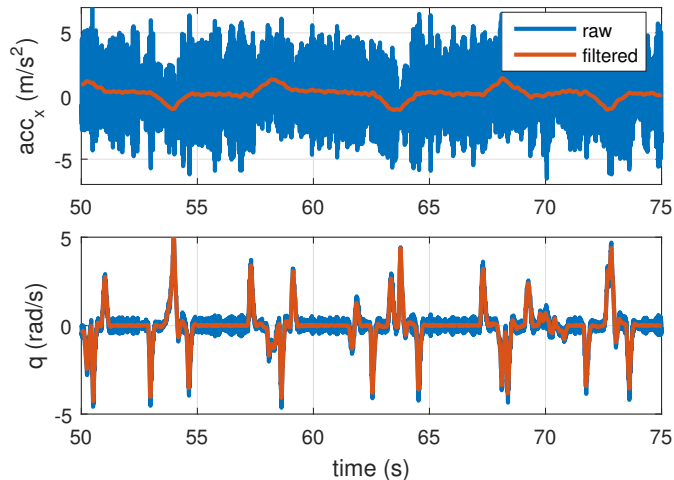


Figure 5: Raw and filtered measurement of the accelerometer and gyroscope. Upper figure shows accelerometer measurements on x axis, while bottom figure shows gyroscope measurement about y axis (pitch rate).

the quadrotor. Since the ideal value of accelerometer measurement, i.e the specific force, indicates the non-gravitational force expressed in the body frame, the horizontal components time the quadrotor mass equal to the aerodynamic force. The vertical component of specific force equals to the sum of real thrust and vertical drag force. The resultant moment can be measured indirectly by recalling Eq 2, with gyroscope measurements and inertia matrix. Since the raw measurements from the Inertia Measurement Units (IMU) are noisy, a 4th order Butterworth filter was used for smoothing. To compensate the lag brought by the low pass filter, data were again filtered in the reversed direction. The selection of cutoff frequency of Butterworth filter is 5Hz and 16Hz for accelerometer and gyroscope respectively, according to the PSD plotted in Fig 4. Butterworth filter shows a satisfactory reduction in noise level as illustrated in Fig 5.

## V. Gray-box Aerodynamic Model

### V.A. Thrust Model

In this section, thrust force of quadrotor is modeled by regarding resultant force on thrust direction as the output. Therefore, thrust discussed in this paper includes both real thrust generated by propellers and drag force acting on the frame and rotors. Thrust model can be derived from  $F_{a,z}$  which stands for the additional aerodynamic force on thrust direction and is mainly caused by a so called thrust variance effect.<sup>8</sup> Generally speaking, thrust from propeller varies as flight speed changes. The preliminary model of  $F_{a,z}$  will be derived from this effect.

In general flight status, for the  $i$ th rotor, the thrust can be modeled as<sup>19</sup>

$$T_i = \frac{\rho abc\omega_i^2 R^3}{2} \left( \frac{\theta_r}{3} + \frac{(u^2 + v^2)\theta_r}{2\omega_i^2 R^2} + \frac{w + \nu_i}{2\omega_i R} \right) \quad (21)$$

where  $a$  is the lift curve slope of blade profile,  $b$  refers to the number of blades,  $c$  is the blade chord,  $R$  indicates the rotor radius,  $\theta_r$  is rotor pitch angle. These parameters are related to rotor design and are all constants for quadrotor. Note here  $\alpha$  equals the angle of attack between coming flow and rotor disk, instead of local angle of attack of blade element.  $\nu_i$  indicates the velocity induced to pass through the rotor plane. Add up four rotors' thrust from Eq 21 and assume air density  $\rho$  remains constant, the total rotor generated thrust is obtained

$$T = \sum T_i = \kappa_1 \sum \omega_i^2 + \kappa_2(u^2 + v^2) + \kappa_3(w + \nu_i) \sum \omega_i \quad (22)$$

Note that we use  $\sum$  instead of  $\sum_{i=1}^4$  for simplicity in the rest of this paper. In hovering flight without ceiling and ground effect, the induced velocity is calculated as

$$\nu_h = \sqrt{\frac{T}{2\rho A}} \quad (23)$$

by substitute  $\nu_h$  and flight speed  $V = 0$  into Eq 22, we can obtain a simple but precise formula of hovering thrust

$$T_h = \kappa_1 \sum \omega_i^2 + \kappa_3 \nu_h w = \kappa_0 \sum \omega_i^2 \quad (24)$$

which also corresponds to the Eq 4. To guarantee that the model works during hovering flight,  $T_h$  is subtracted from the total thrust. The residual

$$T_a = T - T_h = \kappa_2(u^2 + v^2) + \kappa_3(w + \nu_a) \sum \omega_i \quad (25)$$

is named as additional thrust, which represents the thrust variance effect and  $T_a = 0$  holds during hovering. Here  $\nu_a$  stands for the additional induced velocity compared to  $\nu_h$

$$\nu_i = \nu_a + \nu_h \quad (26)$$

Now add  $D_z$  as the aerodynamic drag force on  $z$  direction, the resultant force on  $z$  direction shall be

$$F_z = -T - D_z \quad (27)$$

and recall the definition of  $F_{a,z}$  and  $T_a$ , we have

$$\begin{aligned} F_{a,z} &= -T_a - D_z \\ &= -\kappa_2(u^2 + v^2) - \kappa_3(w + \nu_a) \sum \omega_i - D_z \end{aligned} \quad (28)$$

The model of  $F_{a,z}$  in the form of Eq 28 is derived by summing up the force of individual components, which has the drawback of neglecting interactions between rotors and frame. Another disadvantage of above model is that it's troublesome to compute  $\nu_a$  accurately in different flight conditions, not to mention aerodynamic drag  $D_z$ . An alternative way is to use polynomial function to replace Eq 28

$$F_{a,z} = P_1^3(u, |v|, w) + P_2^3(u, |v|, w) \sum \omega_i \quad (29)$$

where  $P_1^3$  and  $P_2^3$  stand for 3rd order polynomial functions. Compare with Eq 25 and Eq 28,  $P_1^3$  contains the information related to the  $D_z$ ,  $\kappa_2(u^2 + v^2)$  and other complex interaction and coupling aerodynamic forces.  $P_2^3$  is used to fit term  $\kappa_3(w + \nu_a)$ , which is difficult to calculate due to the existence of  $\nu_a$ . Since reduced model of  $F_z$  performs well when speed is zero, it is natural to have  $F_{a,z} = 0$  when airspeed is zero. Obviously, above  $P_1^3$  and  $P_2^3$  fulfill this condition.

Then, the stepwise selection method is used to select regressors from the candidate pool constructed by above four polynomial functions. Flight data for identification ranges from hover to 14m/s flight speed, with all kinds of heading angles. Thus coupling effect will be covered in the model. The selected model structure of  $F_{a,z}$  is

$$F_{a,z} = Z_0 + Z_1 w \sum \omega_i + Z_2 u^2 + Z_3 v^2 + Z_4 u^2 w + Z_5 v w^2 + Z_6 u^2 \sum \omega_i \quad (30)$$

Note that except the bias term  $Z_0$ , other regressors are ordered by selected priority. Terms appears in the front plays more important role than those behind.  $w \sum \omega_i$  term contributes most in thrust variance, which coincides the theoretical model Eq 28. The following terms  $u^2$  and  $v^2$  indicate the importance of horizontal velocity. The last selected  $u^2 \sum \omega_i$  term partially represents the effect of  $\nu_a$  in Eq 28.

After identifying the parameters in above model, we have the model of resultant force on  $z$  direction

$$F_z = \kappa_0 \sum \omega_i^2 + F_{a,z} \quad (31)$$

Since  $F_{a,z}$  is zero while airspeed equals zero,  $\kappa_0$  is able to be estimated during hovering flight.

$\kappa_0$ , and other coefficients for  $F_{a,z}$  are listed in Tab 2, together with  $R^2$  (coefficient of determination) and NRMS (normalized root mean square deviation) quantifying the model performance. Validation and further discussion of this model will be given in the Chapter VI. Note that the unit of velocities is m/s, and rad/s for angular speeds and rotor speeds.

Table 2: Estimation result for  $F_z$  model

Param	$\hat{\Theta}$	$ \hat{\sigma} $	$100 \hat{\sigma}/\hat{\Theta} $
$\kappa_0$	1.58E-6		
$Z_0$	-2.55E-1	5.79E-4	0.23
$Z_1$	9.41E-5	1.05E-7	0.11
$Z_2$	7.39E-3	8.40E-5	1.14
$Z_3$	6.56E-3	1.20E-5	0.18
$Z_4$	2.74E-3	6.37E-6	0.23
$Z_5$	-1.58E-3	6.37E-6	0.40
$Z_6$	2.76E-6	3.02E-8	1.10
$R^2$	0.959829		
NRMS	0.021137		

## V.B. Drag model

$F_x$  and  $F_y$  are forces perpendicular to thrust and often regarded as drag, which are sometimes assumed to be zero in low speed flight. However, for establishing accurate aerodynamic model, the drag force is an issue need

to be considered. The drag force plays significant role and has been researched by several literatures.<sup>9, 15, 16</sup> For a single propeller, the blade flapping phenomenon brings significant effect to drag force.<sup>6, 15</sup> The rotor plane tilts due to flexibility of the rotor and thrust accordingly tilts and bring addition drag.

On the other hand, stiffness always exists, meaning that the additional lift of advancing blade will generate more induced drag than retreating blade. Thus a hub force due to induced drag arises, which is the second component of quadrotor drag force. In addition, vehicle frame also generates aerodynamic drag, including pressure drag and parasite drag, which is related to the square of speed. However, the wind tunnel test shows that the vehicle frame aerodynamic drag is of minor importance, thus is not included when deriving the preliminary model structure. For convenience, the rotor generated drag is expressed in the body coordinate. Simplified but without detectable loss of accuracy, the horizontal drag from each single rotor is summarized as<sup>15</sup>

$$\begin{bmatrix} F_x \\ F_y \end{bmatrix}_i = T_i \left( \frac{1}{\omega_i R} \begin{bmatrix} A_{1c} & (-1)^{(i-1)} A_{1s} \\ (-1)^i A_{1s} & A_{1c} \end{bmatrix} + \begin{bmatrix} d_x & 0 \\ 0 & d_y \end{bmatrix} \right) \begin{bmatrix} u \\ v \end{bmatrix}, i = 1, 2, 3, 4 \quad (32)$$

where  $A_{1c}$ ,  $A_{1s}$  are constants corresponding to blade flapping drag and  $d_x$ ,  $d_y$  are constants for induced drag.  $T_i$  stands for thrust of the  $i$ th rotor. Since drag force on  $z$  direction has been already contained in the thrust model, only forces on  $x$  and  $y$  directions are considered in this section.

Eq 32 contains  $T_i$  and the thrust variance effect increases the difficulty to model drag. As what we did in the previous section, the total thrust is decomposed by

$$T_i = T_{i,h} + T_{i,a} \quad (33)$$

Now add up the drag generated by four rotors. Since the adjacent rotors rotate in different directions, the coupling effect terms which related to  $A_{1s}$  are counteracted. The drag force  $F_x$  can be expressed as

$$F_x = u \sum \left( \frac{\kappa_0}{R} A_{1c} \omega_i + \kappa_0 d_x \omega_i^2 \right) + u \sum (A_{1c} \frac{T_{i,a}}{\omega_i R} + d_x T_{i,a}) \quad (34)$$

In most circumstances, even aggressive flights,  $\omega$  is highly correlated with  $\omega^2$  (the correlation is larger than 0.95). The high collinearity in regressors will largely deteriorate the estimation accuracy of corresponding parameters and potentially lead to large prediction error. An alternative choice is to merge the  $\omega^2$  term into  $\omega$  term. Then Eq 34 can be replaced by

$$F_x = X_1 u \sum \omega_i + P_1^3(u, |v|, w) + P_2^3(u, |v|, w) \sum \omega_i \quad (35)$$

where  $X_1$  is a parameter to be estimated. In the above equation, the  $T_{i,a}$ , related term is replaced by a polynomial function. The polynomial function also contains the mutual effect between rotors and fuselage, which is hard to model accurately using first principle. The effect from minor aerodynamic drag (friction, pressure and parasitic drag) may be also included in this function.

The same data for thrust estimation is used to identify drag model. The model structure is selected as follows

$$F_x = X_0 + X_1 u \sum \omega_i + X_2 |v|w + X_3 u|v| + X_4 uw^2 \sum \omega_i + X_5 uw \sum \omega_i + X_6 uw^2 + X_7 u|v|^2 + X_8 u|v| \quad (36)$$

Tab 3 lists parameters of this model and metrics of performance.

### V.C. Model of Pitch Moment

Moment model was rarely discussed in existing researches. However, during forward flight, reduced model is unable to predict pitching moment accurately. Fig 9c presents the weak prediction performance of reduced model from data acquired in wind tunnel. Due to multiple complex effects acting on the drone, pitch moment model without coupling effect is discussed in this section. Pitch moment with coupling effect may be modeled using more advanced modeling techniques in the future.

There are several effects may bring additional aerodynamic moments. Thrust variance in non hover flights can cause moment variance, thus the coefficient of  $U_q$ , i.e term  $l\kappa_0$  in Eq 24 could change in forward flight. The elastic moment due to blade flapping effect is considered in some literatures (such as Ref. 6, 8), which is approximately proportional to flapping angle and further related to flight speed. The drag

Table 3: Estimation result for  $F_x$  model

Param	$\hat{\Theta}$	$ \hat{\sigma} $	$100 \hat{\sigma}/\hat{\Theta} $
$X_0$	7.47E-2	9.82E-5	0.13
$X_1$	-3.59E-5	1.26E-8	0.03
$X_2$	-6.88E-4	4.17E-6	0.06
$X_3$	-2.00E-3	1.87E-5	0.09
$X_4$	7.79E-9	3.10E-9	39.7
$X_5$	1.83E-6	8.18E-9	0.44
$X_6$	1.15E-3	1.34E-5	1.15
$X_7$	1.62E-4	2.29E-6	1.41
$X_8$	3.28E-5	6.66E-7	2.03
$R^2$	0.99378		
NRMS	0.013510		

force caused moment due to shift between rotor plane and center of gravity is also a main causation of pitch moment. According to the drag model, this moment should be roughly proportional to  $u \sum \omega_i$ . Aerodynamic damping could bring some effect to the model,<sup>1,16</sup> thus pitching rate  $q$  is added as an independent variable. The additional moment caused by multiple rotor interaction, which may bring significant effect, has not been found in existing researches. The frame itself may also brings aerodynamic moments.<sup>5</sup> However, this frame caused pitch moment alters for different types of drones. To sum up, the pitch moment model structure is preliminarily chosen as

$$M_y = b\kappa_0 U_q + P_1^3(u, w, q)U_q + P_2^3(u, w, q) \sum \omega_i + P_3^3(u, w, q) \quad (37)$$

Since  $\kappa_0$  is identified accurately during hover flight, and the rotor distance  $b$  can be measured directly, a difference  $M_{y,a} = M_y - b\kappa_0 U_q$  is used as the output for stepwise structure selection process. Finally, the model structure of pitch moment is determined as

$$\begin{aligned} M_y = & b\kappa_0 U_q + M_0 + M_1 u U_q + M_2 u^2 U_q + M_3 w U_q + M_4 u \\ & + M_5 u^3 + M_6 w + M_7 u w U_q + M_8 q + M_9 u \sum \omega_i + M_{10} u^2 \sum \omega_i + M_{11} u w \end{aligned} \quad (38)$$

From the table,  $U_q$  related terms have higher priority. It signifies that the additional moment mostly comes from the thrust difference between rear and front rotors during forward flight. The least priority regressors selected are those related to  $\sum \omega_i$ , indicating that rotor generate moment is relatively small and the center of gravity is almost within the rotor plane.

The model parameters and metrics are listed in Tab 4.

#### V.D. Model of Yaw Moment

The yaw moment or drag moment is also influenced by aerodynamic effect based on data analysis. Making yaw maneuver during forward flight is quit common for aerial camera in quadrotor configuration. Yaw maneuver is also a main causation of actuator saturation.<sup>7</sup> Thus it is valuable to establish an yaw moment model taking aerodynamic effects into account.

In the reduced model, the rotor inertia  $I_r$  and drag moment coefficient  $\tau$  is required. A parameter estimation can be carried out for estimating them. To avoid effects from translational air flow, yaw maneuvers while hovering is made for identification. However, flight data shows that even in the hovering flight, the reduced model for  $M_z$  is not accurate. Thus by referring Ref. 18, a damping term  $r$  is added to the reduced model. And the yaw moment  $M_z$  in hover flight is then expressed as

$$M_{h,z} = \tau_0 U_r + I_{r,z}(-\dot{\omega}_1 + \dot{\omega}_2 - \dot{\omega}_3 + \dot{\omega}_4) + \gamma r \quad (39)$$

where  $\gamma$  is a damping constant due to rotor generated drag. A least square estimator is used to estimate  $[\tau_0 \quad I_{r,z} \quad \gamma]$ .

Table 4: Estimation result for  $M_y$  model

Param	$\hat{\Theta}$	$ \hat{\sigma} $	$100 \hat{\sigma}/\hat{\Theta} $
$M_0$	1.05E-3	6.47E-5	6.12
$M_1$	-6.53E-9	8.73E-11	1.33
$M_2$	-5.72E-10	1.03E-11	1.80
$M_3$	-3.05E-8	1.92E-10	0.62
$M_4$	-8.42E-3	8.93E-5	1.06
$M_5$	3.59E-5	6.41E-7	1.78
$M_6$	8.67E-3	1.36E-4	1.57
$M_7$	3.08E-9	2.41E-11	0.78
$M_8$	-3.74E-3	2.40E-5	0.64
$M_9$	8.78E-6	4.29E-8	0.48
$M_{10}$	-4.67E-7	4.21E-9	0.90
$M_{11}$	6.69E-4	1.82E-5	2.72
$R^2$	0.958		
NRMS	0.027760		

Next we identify yaw moment  $M_z$  in forward flight cases where additional unknown aerodynamic effects appear. Without priori knowledge for this model based on physical mechanism, we assume that there are two issues affecting the yaw moment, the damping caused by rotation and the influence of the translational speed. Thus the independent variables chosen in the polynomial functions should be  $[u, v, w, r]$ .

Define this additional unknown moment as  $\tilde{M}_z = M_z - M_{h,z}$ , of which the preliminary structure is chosen as

$$\tilde{M}_z = P_1^3(u, v, w, r)U_r + P_2^3(u, v, w, r)\sum \omega_i + P_3^3(u, v, w, r) \quad (40)$$

The first term in Eq 40 is in consideration of variance of coefficient  $\tau_0$  due to translational and rotational speed. The second term with  $\sum \omega_i$  is included because the drag force will cause additional moment in horizontal plane, as we have observed in hover case. And the third term is used to model mutual effect of rotors, moment caused by fuselage, and other unknown effects. After stepwise model structure selection process, the structure in above polynomial functions can be determined. Final model structure of yaw moment is

$$M_z = M_{h,z} + N_0 + N_1v + N_2uU_r + N_3u^3U_r + N_4v^2U_r + N_5uv \quad (41)$$

Parameters of above model, including  $[\tau_0 \quad I_{r,z} \quad \gamma]$ , are listed in Tab 5.

Table 5: Estimation result for  $M_z$  model

Param	$\hat{\Theta}$	$ \hat{\sigma} $	$100 \hat{\sigma}/\hat{\Theta} $
$\tau_0$	1.89E-8	3.83E-11	0.20
$I_{r,z}$	3.34E-6	5.51E-9	0.16
$\gamma$	-9.57E-4	1.45E-5	1.51
$N_0$	5.67E-4	1.02E-5	1.81
$N_1$	-2.18E-4	5.59E-6	2.57
$N_2$	-1.71E-9	1.45E-11	0.84
$N_3$	1.52E-11	1.69E-13	1.10
$N_4$	-8.53E-11	5.52E-13	0.64
$N_5$	-1.10E-4	1.30E-6	1.18
$R^2$	0.977481		
NRMS	0.040945		

The first selected regressor is  $v^2U_r$  instead of  $r$ , which means that the sideslip angle will influence the

efficiency of rotor to generate drag moment. Damping effect is also obvious since regressor  $r$  has high priority, which is in accord with Ref. 18 .The coefficient of  $r$  is negative indicating a damped rotation.

## VI. Model Validation

### VI.A. Validation

The estimated models are validated in this chapter, by predicting the outputs for new sets of flight data.

To further illustrate the performance of model derived in this paper, the reduced model that loses sight of aerodynamic effect is compared.

Fig 6 represent the predicted  $F_z$  and  $F_x$  without wind effect. The forward and backward flight was repeated within a low speed region, in which the aerodynamic effect due to translational speed is relatively small. As expected, the reduced model performs well in this condition. Since gray-box model is based on the concept of thrust variance, when translational speed is small, it should give the same output from reduced model. Fig 7a and Fig 7b present the validation result when flight speed equals 7m/s and 12m/s respectively and the tested quadrotor headed towards the wind flow to maintain a near zero sideslip angle. Obviously, the accuracy of gray-box model is much higher than reduced model. In order to validate the case with aerodynamic coupling between longitudinal and lateral motions, flights with heading angle of 45 degrees were conducted. Fig 8a and Fig 8b present the validation results of 7m/s and 12m/s respectively. Even coupling effect exists,  $F_z$  and  $F_x$  model still have high accuracy.

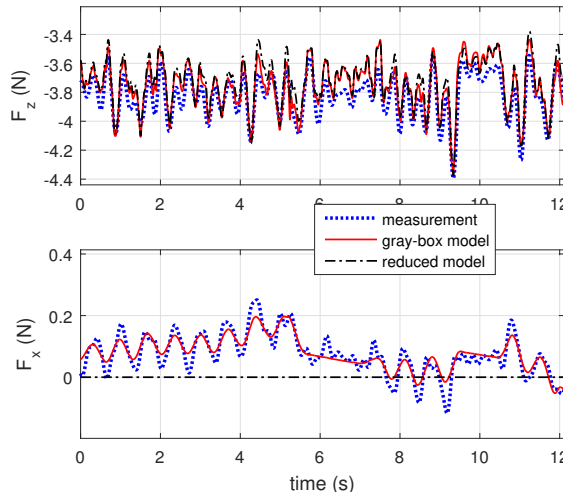


Figure 6: Validation results for the gray-box  $F_z$  and  $F_x$  model during hovering flight, compared with reduced model and measurement value.

The model of pitching moment  $M_y$  was validated using data from zero sideslip angle flights, like those for model estimation. Pitch maneuver without wind effect is shown in Fig 9a. As expected, both reduced model and gray-box model have satisfactory accuracy. However, as flight speed increases to 7m/s and 12m/s, reduced pitch moment model made completely deteriorated prediction. These results are plotted in Fig 9b and Fig 9c. Fig 10 compares residual of the two models in different airspeed using validation data. Besides the accuracy of the gray-box model, the plot shows a nonmonotonic trend of the reduced model residual as airspeed grows. This may be caused by rear rotor effectiveness reduction due to the aerodynamic interaction. To be specific, during a medium speed flight, the rear rotors are disturbed by the wakes from front rotors because the absolute value of angle of attack is relatively small. To maintain the required pitch moment, the rear rotors rotate in a higher speed and then lead the reduced model produce much more negative pitch moment than reality. As flight speed grows, the attitude becomes nose-down to overcome the drag. Then the angle of attack is becoming more negative, and rear rotors are more exposed to the undisturbed coming flow. Since rotors are less influenced, error of reduced model is also reduced in high speed flights. Fig 11 shows the residual of both models versus angle of attack, which could provide evidence of above analysis. The

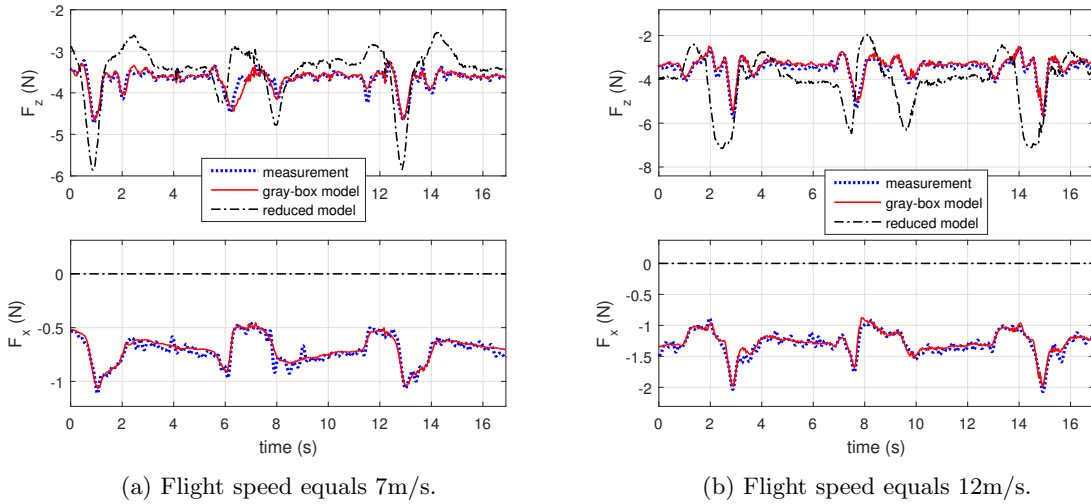


Figure 7: Validation results for the gray-box  $F_z$  and  $F_x$  model in forward flights, compared with reduced model and measurement value.

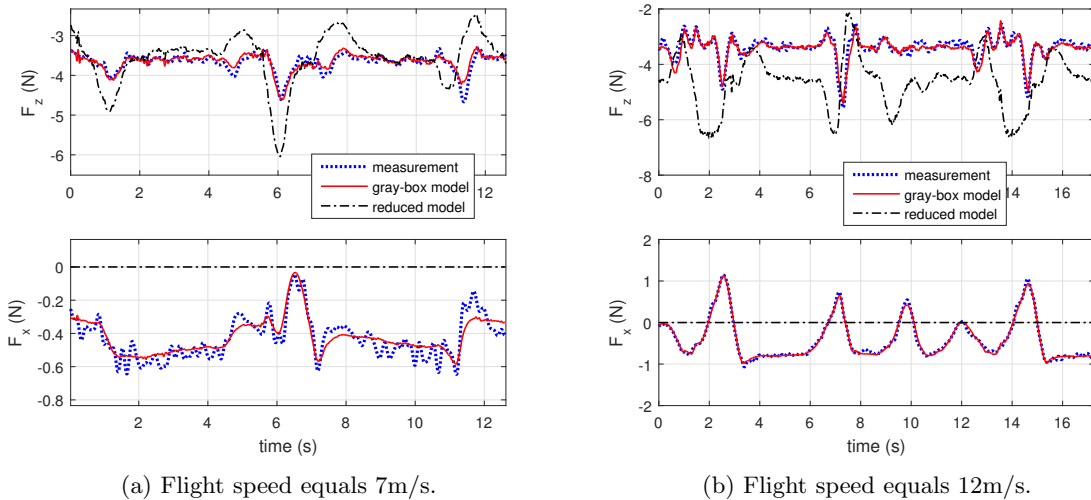


Figure 8: Validation results for the gray-box  $F_z$  and  $F_x$  model in forward flights with 45 deg heading angle, compared with reduced model and measurement value.

reduced model residual and the angle of attack have positive relationship, indicating that the effectiveness of rear rotors increasingly deteriorates as angle of attack increases. With a large positive angle of attack, this phenomenon is so distinct that even gray-box model is unable to completely overcome this model error.

Fig 12 illustrates the validation result of yaw moment  $M_z$  with 0, 7m/s and 12m/s flight speed respectively. Without wind, the gray-box model is more accurate than the reduced model when yaw rate  $r$  is large. When flight speed is non zero, the reduced model gives considerable error compared to the measurement, while gray-box model provides higher predict accuracy. When flight speed is 12m/s, which is closed to the maximum speed of the tested quadrotor, large deviation between reduced model and measurement can be seen. This deviation is positively correlated with the sideslip angle. Since fuselage may bring significant effect on yaw moment model, additional test using quadrotor with smaller fuselage is suggested for studying  $M_z$ .

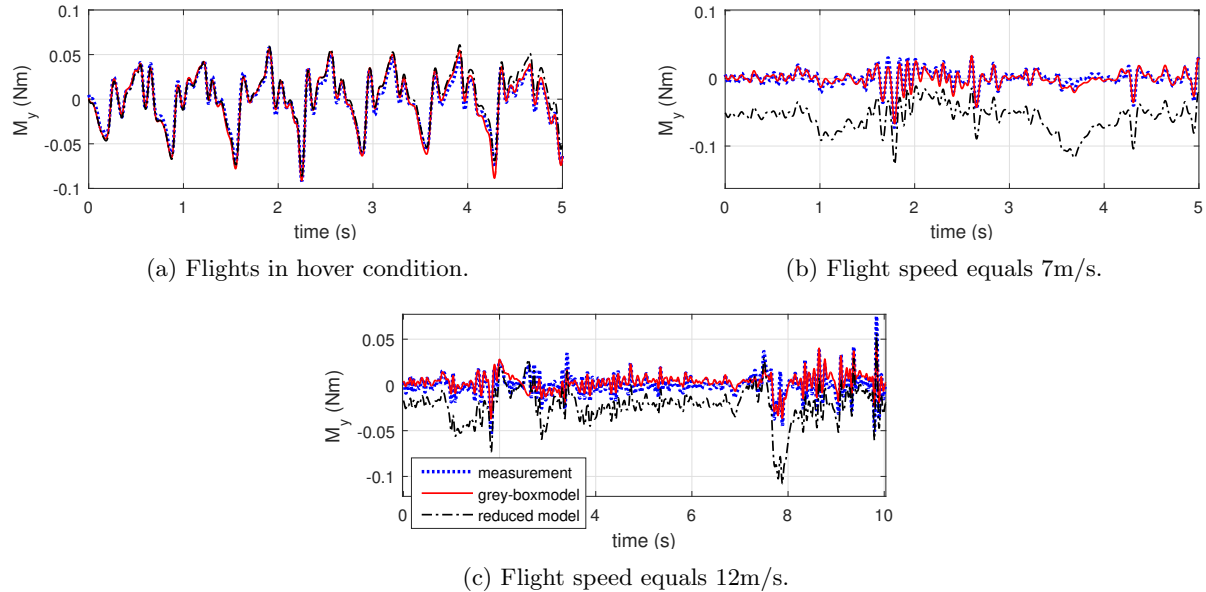


Figure 9: Validation results for the gray-box  $M_y$  model in different flight speeds, compared with reduced model and measurement value.

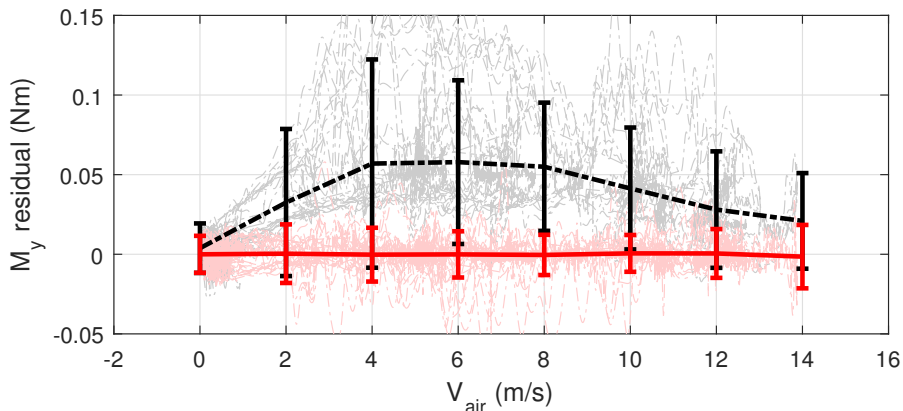


Figure 10: Mean value and  $2 - \sigma$  variance of  $M_y$  model residual in different flight speeds. Rigid red: gray-box model; Dash-dot black: reduced model.

### VI.B. Comparison with First Principle Model Structure

Alternative type of models, which use structures based on first principles, are also computed in comparison with the method used in this paper.

Thrust model with physical structure is compared, which is adopted in Ref. 6, 8, 9, 19 by computing  $\nu_i$  directly. Recall Eq 21, where induced velocity  $\nu_i$  in forward flight is possibly to be computed individually. In our method, the table of dimensionless  $\nu_i$  v.s  $V$  and  $\alpha$  is established based on Glauert formula<sup>12</sup>

$$\bar{\nu}_i^2 = \frac{1}{(\bar{V} \cos \alpha)^2 + (\bar{V} \sin \alpha + \bar{\nu}_i)^2} \quad (42)$$

where  $\bar{\nu}_i$  and  $\bar{\nu}$  are velocities normalized by  $\nu_h$  calculated by Eq 23. Induced velocity corresponding to each data point is estimated by interpolation. Then, the model structure is obtained

$$F_z = a_0 + a_1 \sum \omega^2 + a_2 V^2 \cos^2 \alpha + a_3 (V \sin \alpha + \nu_i) \sum \omega \quad (43)$$

where  $a_0$  to  $a_3$  are parameters which can be estimated using least square method. Fig 14 compares the

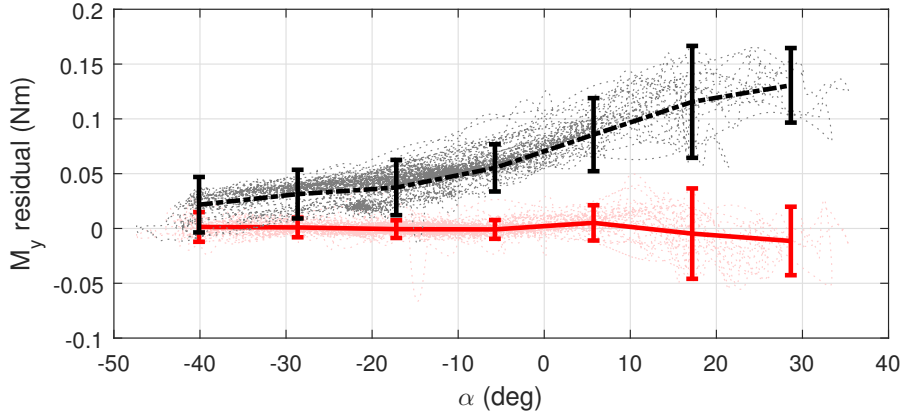


Figure 11: Mean value and  $2 - \sigma$  variance of  $M_y$  model residual in different angles of attack. Rigid red: gray-box model; Dash-dot black: reduced model.

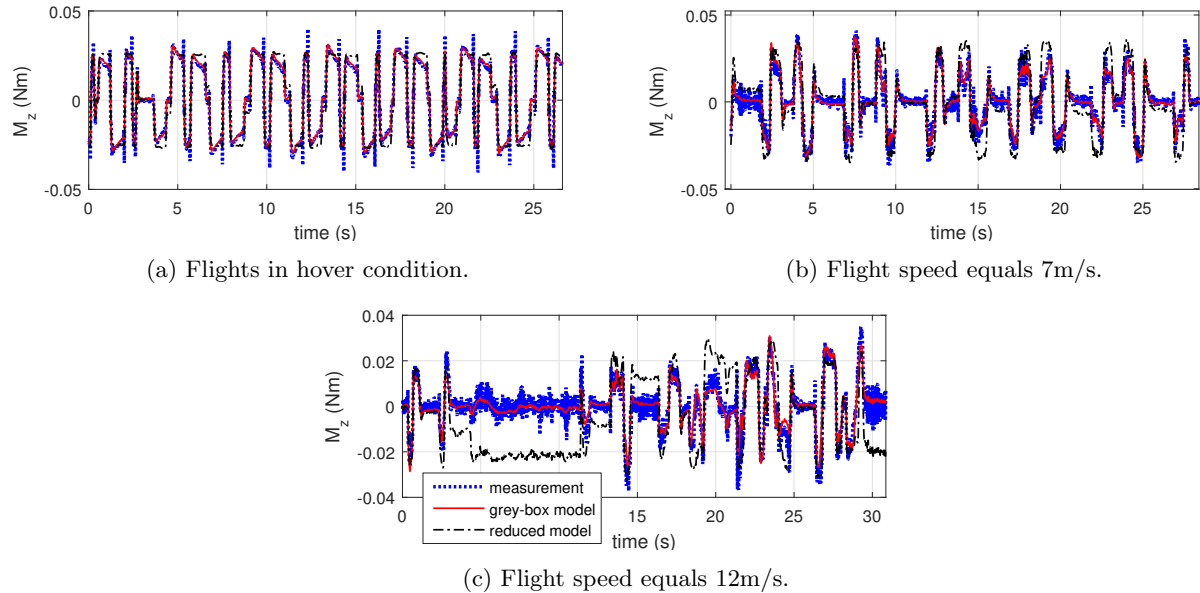


Figure 12: Validation results for the gray-box  $M_z$  model in different flight speeds, compared with reduced model and measurement value.

residuals of two types of models. The width of bar plot indicates the  $2 - \sigma$  boundary of the corresponding region and the center refers to the mean values. Two types of models provide comparable standard error, even though the first principle model ignores the complex interaction between rotors. It means that the induced velocity variance is indeed the mean causation of thrust variance rather than interference in airflow. However, in the flight regime around hovering, the model with physical structure may diverge from the measurement.

As for drag  $F_{a,x}$ , the first term in Eq 35, i.e  $\eta_1 u \sum \omega_i$ , is chosen in the model structure according to Ref. 13, 14, 16. The standard error of two models are comparable as Fig 13 shows. In the low speed region, the mean value of gray-box model is non-zero, which violates the observation. As for the high airspeed regime, the mean value of gray-box model is smaller than the physical structure model.

For yaw moment  $M_z$ , simple structure model expressed as  $M_z = k_0 U_r + k_1 r$  with damping term is adopted in Ref. 18. This model is compared with reduced model and the gray-box model. As Fig 15 shows, with relatively low airspeed, both physical structure model and gray-box model possess high capacity of prediction. As airspeed increases, the model with simple structure gradually diverges from the real measurements while the gray-box model still has relatively high prediction accuracy. Since there are several terms related to  $v$

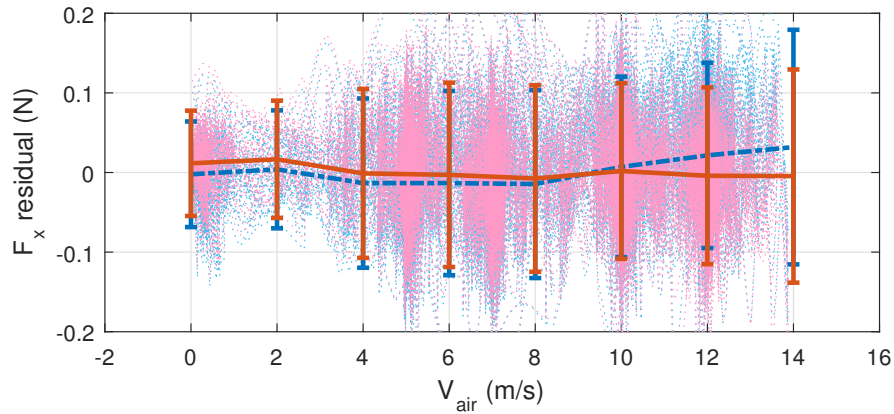


Figure 13: Mean value and  $2 - \sigma$  variance of  $F_x$  model residual. Rigid red: gray-box model; Dash blue: physical structure model.

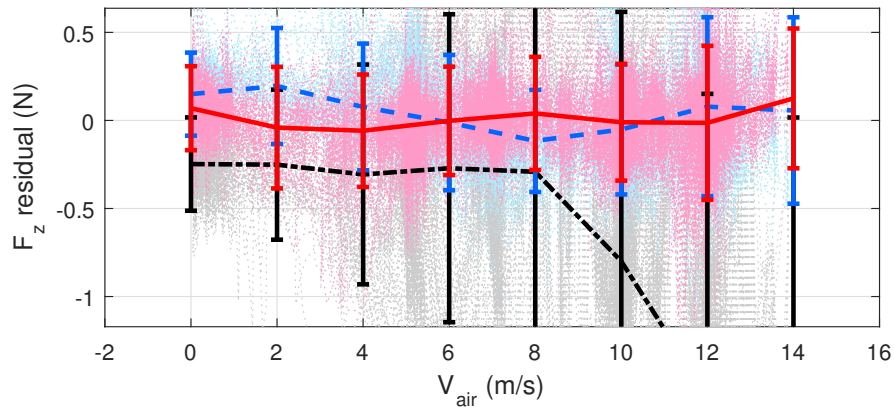


Figure 14: Mean value and  $2 - \sigma$  variance of  $F_z$  model residual. Rigid red: gray-box model; Dash blue: physical structure model; Dash-dot black: reduced model.

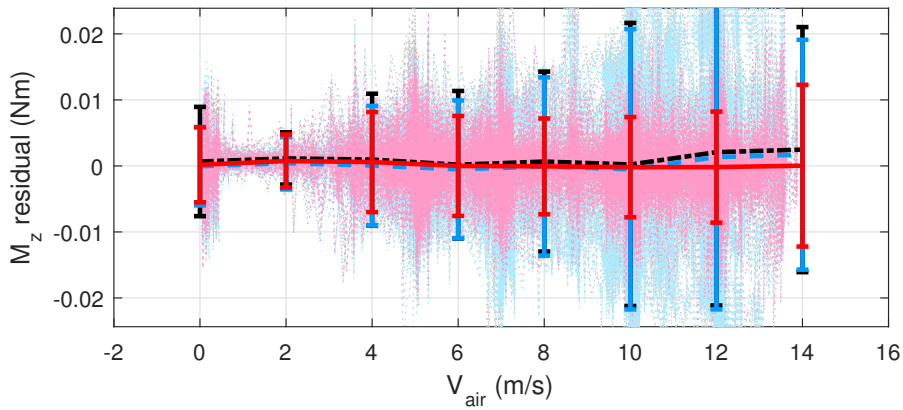


Figure 15: Mean value and  $2 - \sigma$  variance of  $M_z$  model residual. Rigid red: gray-box model; Dash blue: physical structure model; Dash-dot black: reduced model.

in the yaw moment model structure, we may deduce that coupling effect between longitudinal and lateral motions may cause additional yaw moment. Physical meaning of this effect still needs further research.

## VII. Conclusion

In this paper, a gray-box method is presented for modeling quadrotor aerodynamic forces and moments. This gray-box method is based on a-prior knowledge of quadrotor aerodynamics and stepwise structure selection process. Free flight tests in a large diameter open wind tunnel is conducted for model identification and the new model is validated using alternative flight data. Compared with the widely used reduced model, which neglects the aerodynamic force and moments, the gray-box model greatly enhances the prediction ability. The new model is also compared with first principles models from literatures. Estimation and validation results showed that the gray-box model provides better prediction ability than physical model in terms of thrust and moment models, while both are superior to the reduced model.

Moment models are for the first time identified and validated in this paper. The wind tunnel test shows that aerodynamic effects have large influence on pitch and yaw moment. Interactions between rotors are obviously observed. With positive and small negative angle of attack, the effectiveness of rear rotors deteriorates and a higher rotor speed is required to produce the same pitch moment compared to the hover case. An additional yaw moment is also observed, for which the damping effect and the fuselage may play an important role.

Though the gray-box method provides high accuracy, there are still several draw-backs of it. Compared to the physical model, it is less compact and more independent variables are required. This may encourage users to make a trade-off between model accuracy and simplicity. Choice of candidate regressors also affects the model structure of gray-box model. More flexible regressor structure such as multivariate spline functions can be used in the further research for a better performing gray-box model.

## References

- <sup>1</sup>Pierre-Jean Bristeau, Philippe Martin, Erwan Salaün, and Nicolas Petit. The role of propeller aerodynamics in the model of a quadrotor uav. In *Control Conference (ECC), 2009 European*, pages 683–688. IEEE, 2009.
- <sup>2</sup>C.C. de Visser. *Global nonlinear model identification with multivariate splines*. PhD thesis, TU Delft, 2011.
- <sup>3</sup>CC de Visser, J A Mulder, and Qiping Chu. Global nonlinear aerodynamic model identification with multivariate splines. In *AIAA atmospheric flight mechanics conference*, page 5726, 2009.
- <sup>4</sup>Christopher Edwards, Thomas Lombaerts, and Hafid Smaili. Fault tolerant flight control. *Lecture Notes in Control and Information Sciences*, 399, 2010.
- <sup>5</sup>John V Foster and David C Hartman. High-fidelity multi-rotor unmanned aircraft system simulation development for trajectory prediction under off-nominal flight dynamics. In *Air Transportation Integration & Operations (ATIO)–Aerospace Traffic Management (ATM) Conference*, 2017.
- <sup>6</sup>Gabriel M Hoffmann, Haomiao Huang, Steven L Waslander, and Claire J Tomlin. Precision flight control for a multi-vehicle quadrotor helicopter testbed. *Control engineering practice*, 19(9):1023–1036, 2011.
- <sup>7</sup>D.C Höppener. Actuator saturation handling using weighted optimal control allocation applied to an indi controlled quadcopter. 2016.
- <sup>8</sup>Haomiao Huang, Gabriel M Hoffmann, Steven L Waslander, and Claire J Tomlin. Aerodynamics and control of autonomous quadrotor helicopters in aggressive maneuvering. In *Robotics and Automation, 2009. ICRA'09. IEEE International Conference on*, pages 3277–3282. IEEE, 2009.
- <sup>9</sup>Derya Kaya and Ali T Kutay. Aerodynamic modeling and parameter estimation of a quadrotor helicopter. In *AIAA Atmospheric Flight Mechanics Conference*, page 2558, 2014.
- <sup>10</sup>Vladislav Klein, James G Batterson, and Patrick C Murphy. Determination of airplane model structure from flight data by using modified stepwise regression. 1981.
- <sup>11</sup>Vladislav Klein and Eugene A Morelli. *Aircraft system identification: theory and practice*. American Institute of Aeronautics and Astronautics Reston, Va, USA, 2006.
- <sup>12</sup>Gordon J Leishman. *Principles of helicopter aerodynamics with CD extra*. Cambridge university press, 2006.
- <sup>13</sup>Robert C Leishman, John C Macdonald, Randal W Beard, and Timothy W McLain. Quadrotors and accelerometers: State estimation with an improved dynamic model. *IEEE Control Systems*, 34(1):28–41, 2014.
- <sup>14</sup>Teppo Luukkonen. Modelling and control of quadcopter. *Independent research project in applied mathematics, Espoo*, 2011.
- <sup>15</sup>Robert Mahony, Vijay Kumar, and Peter Corke. Multirotor aerial vehicles. *IEEE Robotics and Automation magazine*, 20(32), 2012.
- <sup>16</sup>Philippe Martin and Erwan Salaün. The true role of accelerometer feedback in quadrotor control. In *Robotics and Automation (ICRA), 2010 IEEE International Conference on*, pages 1623–1629. IEEE, 2010.
- <sup>17</sup>AS Mendes, E van Kampen, BDW Remes, and QP Chu. Determining moments of inertia of small uavs: A comparative analysis of an experimental method versus theoretical approaches. In *AIAA Guidance, Navigation, and Control Conference*, page 4463, 2012.
- <sup>18</sup>Mark W Mueller and R. D’Andrea. Stability and control of a quadrocopter despite the complete loss of one, two, or three propellers. In *Robotics and Automation (ICRA), 2014 IEEE International Conference on*, pages 45–52. IEEE, 2014.

<sup>19</sup>Caitlin Powers, Daniel Mellinger, Aleksandr Kushleyev, Bruce Kothmann, and Vijay Kumar. Influence of aerodynamics and proximity effects in quadrotor flight. In *Experimental robotics*, pages 289–302. Springer, 2013.

<sup>20</sup>Ewoud JJ Smeur, Qiping Chu, and Guido CHE de Croon. Adaptive incremental nonlinear dynamic inversion for attitude control of micro air vehicles. *Journal of Guidance, Control, and Dynamics*, 38(12):450–461, 2015.

<sup>21</sup>Ewoud JJ Smeur, Guido CHE de Croon, and Qiping Chu. Gust disturbance alleviation with incremental nonlinear dynamic inversion. In *Intelligent Robots and Systems (IROS), 2016 IEEE/RSJ International Conference on*, pages 5626–5631. IEEE, 2016.

<sup>22</sup>Mark B Tischler. System identification methods for aircraft flight control development and validation. *Advances in Aircraft Flight Control*, pages 35–69, 1996.

<sup>23</sup>Mark B Tischler and Robert K Remple. Aircraft and rotorcraft system identification. *AIAA education series*, 2006.